Mater. Res. Soc. Symp. Proc. Vol. 1224 © 2010 Materials Research Society 1224-FF07-08

Similarity Relationships in Creep Contacts and Applications in Nanoindentation Tests

J.H. Lee,[1] C. Zhou,[1] C.J. Su,[1] Y.F. Gao,[1,2] G.M. Pharr[1,3]

[1] Department of Materials Science and Engineering, University of Tennessee, Knoxville, TN 37996, U.S.A.
[2] Computer Science and Mathematics Division, Oak Ridge National Laboratory, Oak Ridge, TN 37831, U.S.A.
[3] Materials Science and Technology Division, Oak Ridge National Laboratory, Oak Ridge, TN 37831, U.S.A.

ABSTRACT

The study of indentation responses of rate-dependent (viscoplastic or creeping) solids has generally focused on the relationship between indentation hardness and an effective strain rate, which can be defined from a similarity transformation of the governing equations. The strain rate sensitivity exponent can be determined from the slope of a log-log plot of the hardness versus effective strain rate, while determining other constitutive parameters requires a knowledge of the relationship between contact size, shape, and indentation depth. In this work, finite element simulations have shown that the effects of non-axisymmetric contact and crystallography are generally negligible. Theoretical predictions agree well with real nanoindentation measurements on amorphous selenium when tested above glass transition temperature, but deviate quite significantly for experiments on high-purity indium, coarse-grained aluminum, and nanocrystalline nickel. Such a discrepancy is likely to result from the transient creep behavior.

INTRODUCTION

The classic Oliver-Pharr approach to determine the elastic modulus and indentation hardness is based on an analysis of rate-independent elastic-plastic contact, for which the correlation between strain hardening characteristics and indentation responses is well established [1-4]. The study of indentation responses of rate-dependent solids has focused mostly on the concept of an effective strain rate, $\dot{\varepsilon}_{eff}$ [5-11]. For instance, $\dot{\varepsilon}_{eff} = \dot{h}/h$ for pyramidal indenter with indentation depth h, and $\dot{\varepsilon}_{eff} = \dot{a}/D$ for a spherical indenter with contact radius a and indenter diameter D.

Consider a J_2 power-law creeping solid characterized by

$$\sigma/\sigma_0 = \left(\dot{\varepsilon}/\dot{\varepsilon}_0\right)^{1/m}, \text{ or } \dot{\varepsilon} = A\sigma^m, \tag{1}$$

where σ_0 and $\dot{\varepsilon}_0$ are the reference stress and reference strain rate, respectively, m is the stress exponent (reciprocal to the strain rate sensitivity exponent), and $A = \dot{\varepsilon}_0/\sigma_0^m$. As explained by Bower et al. [6], at any particular instant, the strain rates and stresses in a pure creeping solid (i.e., no elasticity and no strain hardening) are independent of the history of loading and depend only on the instantaneous velocities and contact radius prescribed on the surface. Consequently, the strain rate and stress fields are identical to those under a rigid flat punch of radius a which indents a creeping half-space at velocity $\dot{h}$. The geometry of the indenter determines the

relationship between a and h. Apparently, the effective strain rate should be chosen as $\dot{h}/a$, so that

$$\frac{P}{\pi a^2 \sigma_0} = \left(\frac{\dot{h}}{a\dot{\varepsilon}_0} \right)^{1/m} F_a(m), \tag{2}$$

where P is the indentation load, and $F_a(m)$ depends on the stress exponent m and weakly on the friction condition. For a geometrically self-similar indenter, such as cone with half included angle β (e.g., 70.3° for Berkovich-equivalent cone), we have

$$h = \frac{a}{c(m)\tan\beta}, \tag{3}$$

where $c(m)$ depends on the stress exponent m, and also weakly on the friction condition. The dimensionless parameters, $F_a(m)$ and $c(m)$, can be computed from the punch contact problem, which may be further simplified into a nonlinear elastic contact by replacing the strain rates by strains and velocities by displacements in Eq. (1). Finite element simulations using conical indenters, however, indicate a slight dependence of F_a and c on the included angle [10].

Application of the above theoretical predictions, which are derived from axisymmetric contact, to experimental nanoindentation measurements obtained with a Berkovich triangular pyramid needs to take into account effects of the non-axisymmetric contact shape, the difference between $P/\pi a^2$ and the measured hardness, and the crystallographic dependence caused by anisotropies in slip in single crystals. The effects of non-axisymmetric contact and crystallographic dependence are examined by finite element simulations in this work. Comparisons have been made to experiments for amorphous selenium, annealed indium, coarse-grained aluminum, and nanocrystalline nickel. The first material gives $m \approx 1$ when tested above the glass transition temperature. The rest materials give a variation of stress exponent ~4-10.

CONICAL VERSUS BERKOVICH INDENTATION

Nanoindentation measurement techniques typically use the Berkovich indenter, which is a three-sided pyramid with an equivalent cone angle of β=70.3°. The above similarity relationships give

$$\frac{P/\pi a^2}{\sigma_0} = \alpha \left(\frac{\dot{h}/h}{\dot{\varepsilon}_0} \right)^{1/m}, \ \alpha = \frac{F_a(m)}{\left[c(m)\tan\beta \right]^{1/m}}, \tag{4}$$

where the dimensionless parameter α is a monotonically increasing function of m. When m=1, the material is a Newtonian viscous solid and $\alpha = 4/3\tan\beta$ [6]. When $m \to \infty$, the material approaches the rate-independent limit, so that $\alpha = P/\pi a^2 \sigma_0$ is the constraint factor, being about 3 as shown in Fig. 1(a). For rate-independent solids, the true hardness values measured in nanoindentation tests by the Oliver-Pharr approach may be corrected for pile-up and sink-in effects using continuous stiffness measurement techniques and the known elastic modulus. For a rate-independent solid, we define $H_{\text{nominal}} = P/\pi(h\tan\beta)^2$ from the nominal projected contact area, $\pi(h\tan\beta)^2$. Unlike the true hardness, this quantity is experimentally convenient because of its simple relation to the depth of penetration. Consequently,

$$\frac{H_{\text{nominal}}}{\sigma_0}=\alpha^*\left(\frac{\dot{h}}{h\dot{\varepsilon}_0}\right)^{1/m},\ \dot{\varepsilon}_{eff}=\frac{\dot{h}}{h}=BH_{\text{nominal}}^{m}=A\left(\frac{H_{\text{nominal}}}{\alpha^*}\right)^{m},\tag{5}$$

where $\alpha^*=c^2\alpha$. Comparing Eqs. (1) and (5) gives a ratio of $A/B=\alpha^{*m}$, which would allow one to determine the uniaxial creep parameter A from an indentation measurement of B.

Results in Fig. 1(a) are calculated using the available simulation data in Bower et al. [6], which are valid only for blunt indenters (flat-ended punches, or spheres in the limits of small displacement) as validated by our finite element results. For the Berkovich indenter,

$$H_{\text{nominal}}=\alpha_\Delta^* A^{-1/m}\left(\frac{\dot{h}}{h}\right)^{1/m},\ \frac{A}{B}=\alpha_\Delta^{*m},\tag{6}$$

where α_Δ^* can be determined from detailed finite element simulations. Only m=1,2,5 are simulated here. Comparisons in Fig. 1(b) show a negligible contribution of the contact shape to the A/B ratio, which justifies the use of the axisymmetric contact in theoretical studies.

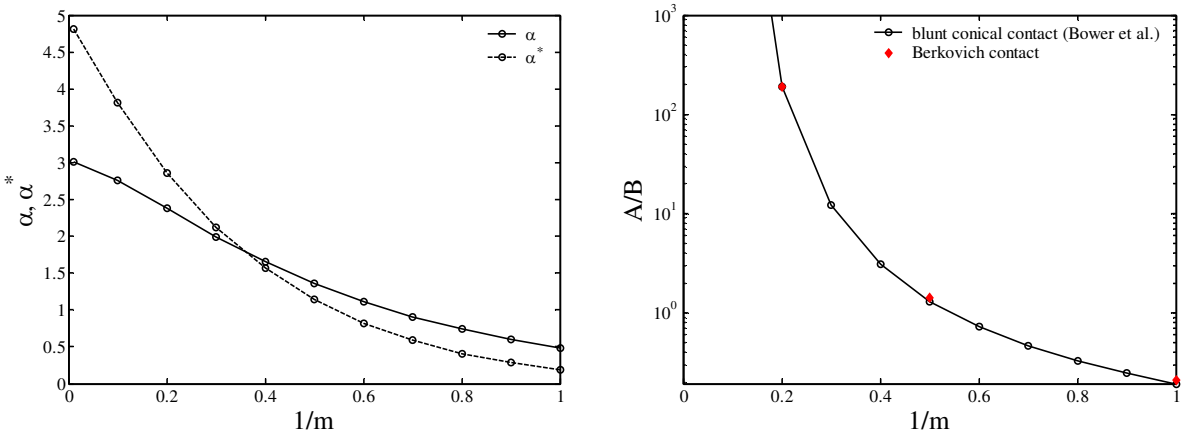

(a) (b)

Figure 1. (a) Dependence of α and α^* on 1/m for Berkovich-equivalent conical contact [6]. (b) The A/B ratio for Berkovich-equivalent conical contact [6] and for Berkovich contact by finite element simulations.

INDENTATION OF CREEPING SINGLE CRYSTALS

Indentation responses of creeping single crystals can be represented in a form similar to Eq. (2). The classic version of crystal plasticity theory in [12,13] is followed in this work. Under infinitesimal deformation conditions, the plastic strain rates are assumed to be a sum of the slip rates over all the slip systems, namely,

$$\dot{\varepsilon}^p=\frac{1}{2}\sum_\alpha \dot{\gamma}^{(\alpha)}\left(s_i^{(\alpha)}m_j^{(\alpha)}+s_j^{(\alpha)}m_i^{(\alpha)}\right),\tag{7}$$

where $\mathbf{s}^{(\alpha)}$ and $\mathbf{m}^{(\alpha)}$ are the slip direction and slip normal on the α-th slip system. The slip rate $\dot{\gamma}^{(\alpha)}$ relates to the resolved shear stress $\tau^{(\alpha)}$ by a power law,

$$\dot{\gamma}^{(\alpha)}=\dot{\gamma}_0\left|\frac{\tau^{(\alpha)}}{\tau_0}\right|^m \operatorname{sgn}\left(\tau^{(\alpha)}\right),\tag{8}$$

where τ_0 is the slip strength, and $\dot{\gamma}_0$ is a reference strain rate. We assume no strain hardening, so that τ_0 is a constant.

For spherical indentation, choosing an effective strain rate, $\dot{\varepsilon}_{eff} = \dot{h}/a$, gives

$$\frac{P}{\pi a^2 \tau_0} = \left(\frac{\dot{h}}{a\dot{\gamma}_0}\right)^{1/m} F_a(m,\mathbf{n}),\ h = \frac{1}{D}\left[\frac{a}{c(m,\mathbf{n})}\right]^2. \tag{9}$$

The constants c and F_a are functions of the material constant m and the crystallographic orientation **n** of the half-space single crystal, and they depend weakly on the interface frictional condition. Eq. (9) can be rewritten as

$$\frac{P}{\pi D^2 \tau_0} = \left(\frac{\dot{h}}{D\dot{\gamma}_0}\right)^{\frac{1}{m}} \left(\frac{h}{D}\right)^{1-\frac{1}{2m}} \Theta, \tag{10}$$

with $\Theta(m,\mathbf{n}) = F_a c^{2-\frac{1}{m}}$. The load-displacement curves from finite element simulations have a transition from elastic to pure creeping responses, as determined by comparing Eq. (10) to the elastic response:

$$\frac{P_{elastic}}{\pi D^2 \tau_0} = \frac{4}{3\sqrt{2}} \frac{E^*}{\pi \tau_0} \left(\frac{h}{D}\right)^{\frac{3}{2}}. \tag{11}$$

The effective indentation modulus E^* can be calculated from the elastic constants and **n** [3]. Similar representations can be found for conical indentation, leading to the same orientation dependence function Θ in

$$\frac{P}{\pi h^2 \tau_0} = \left(\frac{\dot{h}}{h\dot{\varepsilon}_0}\right)^{\frac{1}{m}} (\tan\beta)^{2-\frac{1}{m}} \Theta,\ \frac{P_{elastic}}{\pi h^2 \tau_0} = \frac{4}{\pi^2} \tan\beta \frac{E^*}{\tau_0}. \tag{12}$$

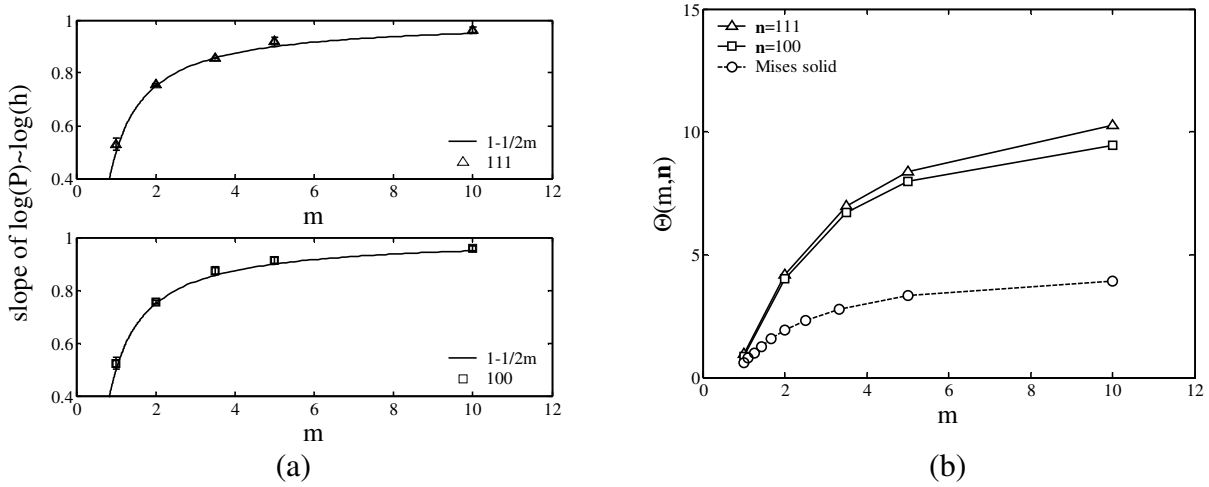

Figure 2. For spherical indentation on single crystals with $\dot{h} = const$, the slope of $\log(P) \sim \log(h)$ and the function Θ are plotted against the material constant m in (a) and (b), respectively. Two representative surface orientations are shown, **n**={111} and {100}.

The above predictions have been validated by finite element simulations. The ABAQUS User-defined Material subroutine in [12] was modified according to the constitutive law

specified in Eqs. (7) and (8). For a spherical indentation at a constant $\dot{h}$, the slope of a log-log plot of the load-displacement curve is predicted as $1-1/2m$, as confirmed by numerical results in Fig. 2(a). Results in Fig. 2(b) suggest that a plateau value is reached when m is about 10. Fig. 3 shows a variation of Θ of about 7% according to the contours plotted on the standard [001] triangle. The dependence on the indentation direction is thus weak for fcc single crystals because of the existence of many slip systems. Recent nanoindentation tests on coarse-grained aluminum specimens [14] seem to support this conclusion, since no noticeable variations except for experimental errors have been found when indenting various grains.

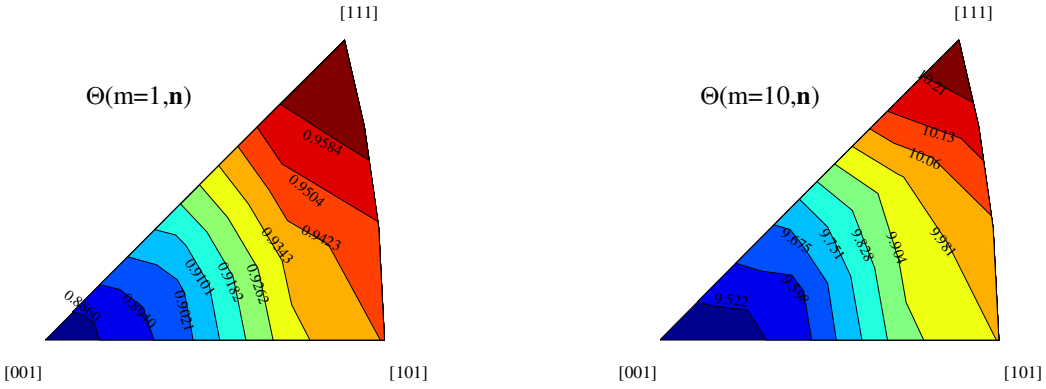

(a) (b)

Figure 3. Contours of Θ, as plotted on the [001] inverse pole figure, show the dependence on surface normal for spherical indentation with constant $\dot{h}$: (a) m=1, (b) m=10.

EXPERIMENTAL COMPARISONS

The predicted A/B ratio has been compared to a number of experimental results. For amorphous selenium tested above the glass transition temperature (displaying a Newtonian viscous flow behavior and $m \approx 1$), the measured value is found to be $A/B \approx 0.256$ [7,9], while the predicted value is about 0.21 as shown in Fig. 1. For high-purity indium, Lucas and Oliver [8] found that $m \approx 7$ and $A/B > 10^5$. It should be noted that A/B goes to infinity as m increases from unity to infinity, as shown in Fig. 1. When using $\alpha^* = (A/B)^{1/m}$, we found that the experimental result gives $1.4 < \alpha^* < 1.7$, which is much less than the predicted α^* (about 3 in Fig. 1). A similar discrepancy is also noted in a recent work on nanocrystalline nickel [15], giving experimentally $m \approx 5$ and $\alpha^* \approx 1.4$, which again is much less than the predicted α^* (about 2.8 in Fig. 1). A close examination of these experiments suggests that this discrepancy might be due to the transient creep behavior. In the range of m values in [8,14,15], a pile-up is predicted while experimental observations show sink-in, which is a result of strain hardening behavior. The pure-creeping constitutive law in Eq. (1) is unable to describe this behavior, and more advanced analyses (e.g., [16]) are needed along this line.

SUMMARY

In summary, the correlations of contact pressure, effective strain, and effective strain rate in the indentation responses of creeping solids have been analyzed theoretically by a similarity approach and numerically by finite element simulations. The stress exponent (reciprocal to the strain rate sensitivity exponent) can be accurately determined, but other parameters, as indicated by the A/B ratio in Eqs. (1), (5), and (6), only agree with theoretical predictions when $m \to 1$. This discrepancy is likely to result from the strain hardening behavior in primary creep, while the theoretical predictions are limited to steady-state creep. These details may be important in using indentation creep data to measure and predict uniaxial creep constants used in material design.

ACKNOWLEDGEMENTS

Financial support for this work was provided by the National Science Foundation under grant number CMMI 0800168. JHL was supported by Agilent Technologies, the Center for Materials Processing at the University of Tennessee, and the Korea Research Foundation Grant (KRF-352-D00001) funded by the Korean Government (MOEHRD). Research at the Oak Ridge National Laboratory was sponsored by the Division of Materials Sciences and Engineering, Office of Basic Energy Sciences, US Department of Energy, under contract DE-AC05-00OR22725 with UT-Battelle, LLC.

REFERENCES

1. W.C. Oliver and G.M. Pharr, *J. Mater. Res.* **7**, 1564 (1992).
2. W.C. Oliver and G.M. Pharr, *J. Mater. Res.* **19**, 3 (2004).
3. Y.F. Gao and G.M. Pharr, *Scripta Mater.* **57**, 13 (2007).
4. Y.F. Gao, H.T. Xu, W.C. Oliver, and G.M. Pharr, *J. Mech. Phys. Solids* **56**, 402 (2008).
5. M.J. Mayo and W.D. Nix, *Acta Metall.* **36**, 2183 (1988).
6. A.F. Bower, N.A. Fleck, A. Needleman, and N. Ogbonna, *Proc R Soc London A* **441**, 97 (1993).
7. W.H. Poisl, W.C. Oliver, and B.D. Fabes, *J. Mater. Res.* **10**, 2024 (1995).
8. B.N. Lucas and W.C. Oliver, *Metall. Mater. Trans. A* **30**, 601 (1999).
9. J.A. LaManna, PhD Thesis, University of Tennessee (2006).
10. S.J. Sohn, PhD Thesis, University of Tennessee (2007).
11. F.X. Liu, Y.F. Gao, and P.K. Liaw, *Metall. Mater. Trans. A* **39**, 1862 (2008).
12. Y. Huang, Mech. Rep. 178, Division of Applied Science, Harvard University (1991).
13. J.W. Kysar, *J. Mech. Phys. Solids* **49**, 1099-1128 (2001).
14. C.J. Su, et al., unpublished experimental results (2009).
15. C. L. Wang, Y.H. Lai, J.C. Huang, and T.G. Nieh, *Scripta Mater,* **62**, 175 (2010).
16. N. Ogbonna, N.A. Fleck, A.C.F. Cocks, *Int. J. Mech. Sci.*, **37**, 1179 (1995).